Homogeneity of a Supersaturated Solid Solution

J. H. He,[1] H.W. Sheng,[1] J. S. Lin,[2] P. J. Schilling,[3] R. C. Tittsworth,[4] and E. Ma[1,*]

[1]*Department of Materials Science and Engineering, The Johns Hopkins University, Baltimore, Maryland 21218*
[2]*Solid State Division, Oak Ridge National Laboratory, Oak Ridge, Tennessee 37830*
[3]*Department of Mechanical Engineering, University of New Orleans, New Orleans, Louisiana 70145*
[4]*Center for Advanced Microstructures and Devices, Louisiana State University, Baton Rouge, Louisiana 70803*

(Received 10 April 2002; published 3 September 2002)

Extended x-ray absorption fine structures, small-angle x-ray scattering, and atomistic model calculations have been employed to probe the homogeneity of the fcc solution created in Ag-Cu, a classical system demonstrating the extension of solubility across the entire miscibility gap through rapid quenching. Our results reveal that in many cases the supersaturated solutions formed have decomposition features on the scale of 1 nm. Conventional diffraction methods are inadequate in determining the level of supersaturation or the uniformity of such solid solution alloys.

DOI: 10.1103/PhysRevLett.89.125507 PACS numbers: 61.43.Dq, 61.20.Ja, 61.25.Mv, 64.60.My

Rapid quenching from either the liquid or the vapor phase has been widely used to produce nonequilibrium alloys. Duwez and co-workers' early work on liquid-quenched alloys, including those in the eutectic Ag-Cu system, was a classical example in this regard [1,2]. Since then, single-phase, supersaturated, solid solutions have been claimed to form in this and a large number of other positive-heat-of-mixing systems through rapid quenching or even solid-state routes [3–21]. The alloys obtained are believed to be compositionally homogeneous. This is because the very high effective quench rates experienced by the samples, especially in the case of vapor deposition using substrates held at subambient temperatures, are thought to lead to kinetic constraints so severe that they would render chemical partitioning utterly impossible. Such "polymorphic constraints" [22,23] are in fact often used to explain phase selection during rapid quenching as well as during externally driven alloying (such as mixing by ion irradiation or plastic deformation [8,10]). In terms of experimental proof, x-ray or electron diffraction data constitute the main source of evidence. In the Ag-Cu case, a set of fcc peaks are shifted away from the Ag and Cu positions, which is fairly consistent with the lattice parameter predicted by Vegard's law. Such a single set of Bragg peaks in lieu of those from the two constituent elements is generally regarded as indicative of homogeneous supersaturation without phase separation.

However, the exact nature of the nonequilibrium alloys created deep inside the miscibility gap is in fact not well established, as there has been little systematic work characterizing the atomic-level structures. Recently, calculations using a multilayer model [24] have shown that a coherent microstructure composed of compositionally modulated layers on a nanometer scale can in itself also lead to a set of Bragg peaks appearing at the positions corresponding to the average lattice parameter of the two pure elements, even when no such lattice parameter is physically present inside the sample [24]. It is therefore of interest to understand exactly what kind of alloys are created between the otherwise immiscible elements by rapid quenching, and to examine in detail the extent of (spinodal) decomposition and clustering [25,26], if they have not been suppressed. In this Letter, we use a combination of extended x-ray absorption fine structures (EXAFS), small-angle x-ray scattering (SAXS), and calculations based on atomistic simulations to probe the short to intermediate range structures and the uniformity of a supersaturated Ag-Cu solution.

$Ag_{50}Cu_{50}$ foils with thickness up to 5 μm were prepared using dc sputter deposition of a composite target onto liquid nitrogen cooled glass substrates at an Ar pressure of 5 mTorr in a system with a base vacuum of 1×10^{-8} Torr. The deposition using a cryogenic substrate, in lieu of a room temperature (RT) substrate or liquid quenching, is usually believed to be farther away from equilibrium and often taken for granted to produce homogeneous alloys. The sputtering power was varied in the current range of 60–120 mA at 300 V. Figure 1 displays the XRD (x-ray diffraction) pattern of the as-deposited (80 mA) $Ag_{50}Cu_{50}$ as an example, showing dominant (111) and (222) reflections indicating pronounced texturing. The (111) peak appears at a position in between those of elemental Ag and Cu, with a nearly symmetric shape that can be reasonably well fit using a Lorentz function (Fig. 1 inset). The estimated lattice parameter of 3.88 Å is only slightly larger than the Vegard's law prediction (3.85 Å) [2,13]. These features are often taken as the proof of the formation of a homogeneous fcc solution with the nominal overall composition.

However, SAXS measurements of these samples, conducted with a sample-to-detector distance of 1.119 m [27], revealed a broad peak for a range of sputtering power (current), as shown in Fig. 2. The appearance of this maximum in SAXS suggests possible compositional modulations, with a wavelength of $L = 2$–3 nm, i.e., the presence of Ag (or Cu) enriched and depleted domains with sizes of the order of $\sim$1 nm. Nonuniformity on such

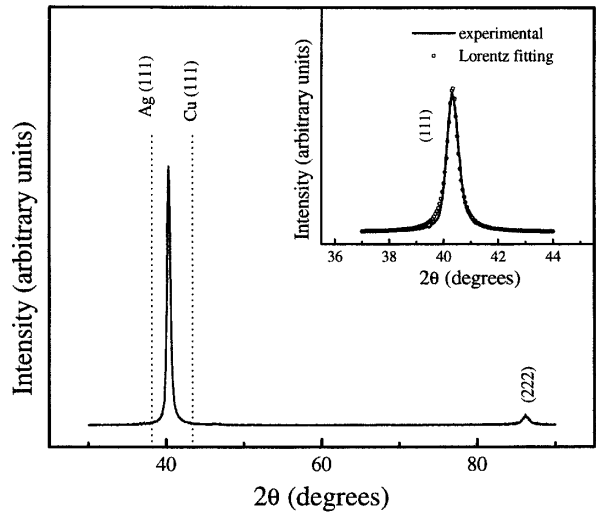

FIG. 1. XRD pattern of the $Cu_{50}Ag_{50}$ film sputter deposited at 80 mA. The inset is the fit to the (111) peak using the Lorentz function, showing the fairly symmetric shape of the peak. Note the peak shift relative to those of pure Ag and Cu (dotted lines).

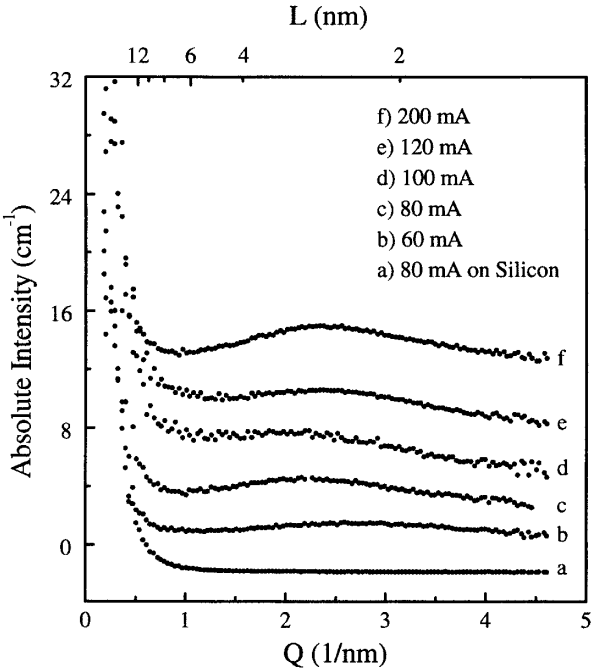

FIG. 2. Small-angle x-ray scattering spectra for the $Cu_{50}Ag_{50}$ alloy films deposited on glass substrate with different sputtering currents. The presence and intensity of the scattering maximum is dependent on deposition conditions. For comparison, an apparently more homogeneous $Cu_{50}Ag_{50}$ film deposited at a current of 80 mA on Si substrate is also included (spectrum *a*). $Q = 4\pi \sin\theta/\lambda$, where θ = half the scattering angle and λ is the wavelength of the Cu $K\alpha$ x ray. The composition modulation wavelength can be estimated using $L = 2\pi/Q$. For clarity of comparison, the scattering curves are vertically shifted by an arbitrary factor with respect to curve *b*.

a scale can also be studied using the local environment probe, EXAFS. Transmission Cu *K*-edge EXAFS measurements were performed at RT at the LSU electron storage ring (1.3 GeV, 180 mA) with the x-ray beam monochromatized using Si (220) double crystals. The phase-corrected Fourier-transformed EXAFS of the $Cu_{50}Ag_{50}$ film deposited at 80 mA is shown in Fig. 3(a), in comparison with that of a pure Cu foil. Data fitting (see below) and simulations of the Fourier transforms indicate that the first (two) split peaks for $Cu_{50}Ag_{50}$ are mainly from Cu-Cu and Cu-Ag paths within the nearest neighbor (NN) shell, respectively, and the next major peak is from several single or multiple scattering paths beyond the NNs. The NN Fourier transform in the range of 1.8–3.5 Å was inverse-Fourier transformed with the k^2 weighting factor. Fitting using the FEFF8 theory [28,29] in the single scattering approximation was performed in the inverse-Fourier space range of 2.5–12.0 Å^{-1} using the FEFFIT code [30]. The EXAFS is given by [31]

$$\chi(k) = \sum_j \frac{S_0^2 N_j}{kR_j^2} f_j(k) e^{-2k^2\sigma_j^2} e^{2R_j/\lambda} \sin[2kR_j + \phi_j], \quad (1)$$

where S_0^2 is an amplitude reduction factor that can be obtained through analyzing the EXAFS of the Cu foil [32]. R_j is the averaged distance of the jth scattering path, N_j is the coordination number (CN) constrained to be 12 for the fcc structure, and $f_j(k)$ is the effective scattering amplitude. ϕ_j is the phase shift, λ is the photon electron's mean free path, and σ_j^2 is the Debye-Waller factor.

The match with experimental EXAFS achieved through fitting is shown in the *k*-space plot of Fig. 3(b). Table I presents the resultant NN structural parameters. The Cu-Cu pairs dominate, with an average Cu CN of 7.0 ± 0.4. The degree of clustering can be characterized using the Warren-Cowley chemical short-range order parameter $\alpha = 1 - (N_{AB}/NC_B)$, where N_{AB} is the NN CN of B atoms around an A atom, N is the total CN in the NN shell, and C_B is the atomic concentration of B. Positive and negative deviations from zero indicate clustering and ordering, respectively. This $Ag_{50}Cu_{50}$ alloy shows a positive $\alpha = 0.17 \pm 0.07$, suggesting clustering/phase separation. Because all the samples were warmed up to RT and characterized the same way and yet showed different degrees of decomposition (Fig. 2), the latter must have occurred mostly during deposition. The bond length of Cu-Ag (2.69 ± 0.01 Å) is larger than Cu-Cu (2.62 ± 0.04 Å), suggesting that bond lengths relax in the alloy to different values and the lattice is distorted relative to the average fcc sites for energy reduction [33,34]. The Debye-Waller factors of $Cu_{50}Ag_{50}$ are much larger than Cu, due to a larger degree of disorder and vibration in the alloy, resulting in the strong amplitude reduction seen in Fig. 3.

The SAXS and EXAFS results above point to the inadequacy and insensitivity of XRD in revealing and characterizing the degree of (spinodal) decomposition, as further supported by the following simulations. A series of partially decomposed states in an fcc lattice were first constructed using Monte Carlo (MC) simulations with

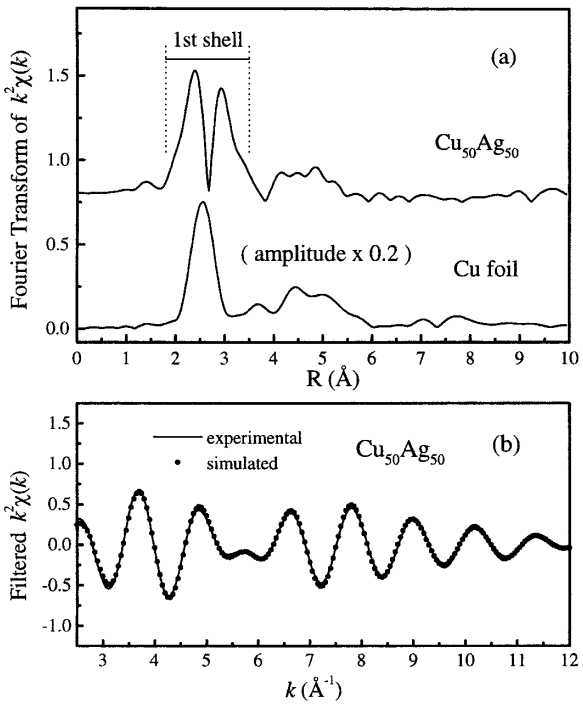

FIG. 3. (a) Phase-corrected Fourier transform of the Cu K-edge EXAFS of the $Cu_{50}Ag_{50}$ alloy film, compared with that of elemental Cu foil. The data were transformed using k^2 weighting in the range of 2.5–12.0 $Å^{-1}$. (b) $k^2\chi(k)$ fit of EXAFS in inverse-Fourier transformed space in the range 2.5–12.0 $Å^{-1}$. The solid and dotted curves are from the experiment and the fit, respectively.

the Ising model and Kawasaki direct exchange mechanism [35]. For simplicity, the Hamiltonian of the system is chosen as $H = -J\sum S_i S_j$, where J is the energy of an A-B pair, $\langle i, j\rangle$ denotes only NN interactions, and S_i takes the values of 1 and -1 representing A or B atoms, respectively. The MC simulations were performed in an fcc lattice of 16 384 sites ($16 \times 16 \times 16$ fcc cells) with $A : B = 1$ at a temperature of $T/T_C = 0.7$ (the critical temperature $T_C = 1385$ K). The phase-separating MC configurations, after scaling the lattice parameter to follow Vegard's law, were further relaxed with molecular dynamics (MD) simulations at 300 K using a quantum Sutton-Chen force field [36] and then were used to calculate the XRD spectra using the Debye scattering formula [37]

$$I = \sum_j^N f_j^2 + \sum_j \sum_{k \neq j} f_j f_k \frac{\sin 2\pi s r_{jk}}{2\pi s r_{jk}}, \qquad (2)$$

where f_j is the tabulated scattering factor of atom j, r_{jk} is the distance between atoms j and k, and $s = 2\sin\theta/\lambda$ is the scattering vector. To reduce the peak broadening effect due to small system size, larger systems comparable to the grain size in deposited films ($\sim$ 13 nm) were used in the XRD calculations.

Figure 4 shows the MC/MD configurations at different stages of decomposition and the corresponding XRD spectra. The domain size increases with decomposition (e.g., of the order of 1 and 2 nm for the Cu-rich domains at $\alpha = 0.25$ and 0.41, respectively). Apparently, XRD cannot "see" the decomposition until a shoulder begins to appear at the first peak at $\alpha = 0.25$. In the early stage of decomposition, the domains are so fine (1–2 nm) that coherency is maintained to a large extent, a scenario similar to the Au-Ni case for modulation wavelengths below about 3 nm [38]. These fine modulations will then produce diffraction peaks at the positions corresponding to the average lattice parameter of the regions sampled within the coherence length [24]. As such, XRD will not be able to distinguish a (partially) phase-separating solution from a truly uniform one.

In summary, we processed $Cu_{50}Ag_{50}$ under conditions that are usually believed to be sufficient to quench-in a homogeneous random solid solution. While XRD indeed suggests such a uniform alloy, phase separation has actually occurred on a nanoscale and the degree of (spinodal) decomposition in Ag-Cu is sensitive to the sample preparation conditions (Fig. 2). EXAFS analysis of a model case reveals that the alloy is characterized by a positive α of 0.17 ± 0.07. The corresponding domain size of $\sim$1 nm as suggested by MC/MD simulations is consistent with the modulation wavelength estimated from SAXS. Different bond lengths due to relaxation were observed through EXAFS and in MC/MD configurations. Our simulations support the experimental finding that XRD is not able to detect decomposition in its early stages. While truly homogeneous superaturated solutions may be achievable through adjusting the quenching conditions [39,40] (e.g., Ag-Cu deposited on Si, Fig. 2), many

TABLE I. Structural parameters obtained from EXAFS fitting.

Pair correlations	Coordination number	Bond distance (Å)	σ^2_{300K} ($Å^2$)
fcc Cu foil			
Cu-Cu	12	2.54 ± 0.01	0.008 ± 0.001
Sputtered $Cu_{50}Ag_{50}$			
Cu-Cu	7.0 ± 0.4	2.62 ± 0.04	0.024 ± 0.002
Cu-Ag	5.0 ± 0.4	2.69 ± 0.01	0.014 ± 0.001

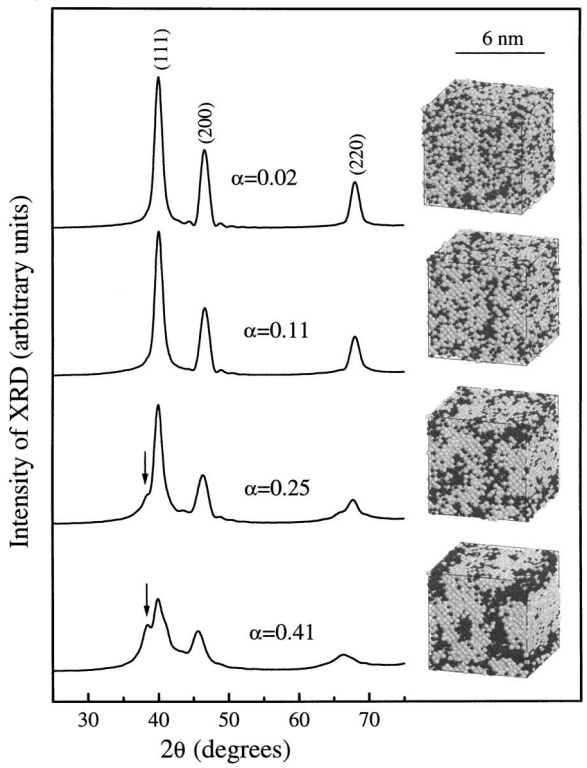

FIG. 4. MC/MD configurations of $Cu_{50}Ag_{50}$ at different staes of spinodal decomposition are shown in the right column. The left column displays the corresponding calculated XRD patterns. The smaller darker balls are Cu atoms.

presumably homogeneous alloys obtained so far inside miscibility gaps under the assumption of polymorphic constraints are likely to have undergone (incipient or partial) phase separation on ultrafine scales that escaped detection. The composition modulations on the scale of 1 nm are difficult to image through-foil in an electron microscope. These ultrafine scales are understandable as the alloys are severely undercooled to far below T_C where driving forces for unmixing are large and diffusion kinetics are very limited. The spinodal decomposition waves may be controlled to form desired patterns in thin films. It is not possible to rely on diffraction methods to determine the true level of supersaturation or the homogeneity of a solid solution.

The authors thank Dr. C. L. Chien for his interest and generous help. This work was funded by the National Science Foundation, Grant No. DMR-0080361 and by Grant No. DOE DE-AC05-00OR22725 at ORNL.

*Corresponding author.
Electronic address: ema@jhu.edu

[1] W. Klement, R. H. Willens, and P. Duwez, Nature (London) **187**, 869 (1960).
[2] P. Duwez, R. H. Willens, and W. Klement, J. Appl. Phys. **31**, 1136 (1960).
[3] R. K. Linde, J. Appl. Phys. **37**, 934 (1966).
[4] S. Mader, A. S. Nowick, and H. Widmer, Acta Metall. **15**, 203 (1967).
[5] C. N. J. Wagner *et al.*, J. Appl. Phys. **39**, 3690 (1968).
[6] B. Cantor and R.W. Cahn, Scr. Metall. **10**, 381 (1976); Acta Metall. **24**, 845 (1976).
[7] B. Y. Tsaur and J.W. Mayer, Appl. Phys. Lett. **36**, 823 (1980).
[8] L. C. Wei and R. S. Averback, J. Appl. Phys. **81**, 613 (1997).
[9] R. Najafabadi *et al.*, J. Appl. Phys. **74**, 3144 (1993).
[10] T. Klassen, U. Herr, and R. S. Averback, Acta Mater. **45**, 2921 (1997).
[11] F. Wu *et al.*, Acta Mater. **49**, 453 (2001).
[12] Z. H. Barber, Vacuum **41**, 1102 (1990).
[13] N. Saunders and A. P. Miodownik, J. Mater. Sci. **22**, 629 (1987).
[14] C. Michaelson, C. Gente, and R. Bormann, J. Appl. Phys. **81**, 6024 (1997).
[15] H. Rizzo *et al.*, Metall. Trans. A **25**, 1579 (1994).
[16] H. Y. Bai *et al.*, Phys. Rev. B **63**, 4202 (2001).
[17] R. Busch *et al.*, Acta Metall. Mater. **44**, 2567 (1996).
[18] J. H. He *et al.*, Phys. Rev. Lett. **86**, 2826 (2001).
[19] J. H. He and E. Ma, Phys. Rev. B **64**, 144206 (2001).
[20] R. P. van Ingen, R. H. J. Fastenau, and E. J. Mittemeijer, Phys. Rev. Lett. **72**, 3116 (1994).
[21] H. U. Krebs and M. Störmer, Phys. Rev. Lett. **75**, 3966 (1995).
[22] W. L. Johnson, Prog. Mater. Res. **30**, 81 (1986).
[23] E. Ma and M. Atzmon, Phys. Rev. Lett. **67**, 1126 (1991).
[24] C. Michaelsen, Philos. Mag. A **72**, 813 (1995).
[25] V. Ozolins, C. Wolverton, and A. Zunger, Phys. Rev. B **57**, 6427 (1998).
[26] C. Wolverton, V. Ozolins, and A. Zunger, Phys. Rev. B **57**, 4332 (1998).
[27] G. D. Wignall, J. S. Lin, and S. Spooner, J. Appl. Crystallogr. **23**, 241 (1990).
[28] A. L. Ankudinov *et al.*, Phys. Rev. B **58**, 7565 (1998).
[29] A. L. Ankudinov and J. J. Rehr, Phys. Rev. B **62**, 2473 (2000).
[30] M. Newville *et al.*, Physica (Amsterdam) **208B&209B**, 154 (1995).
[31] E.A. Stern and S.M. Heald, in *Handbook on Synchrotron Radiation*, edited by E. E. Koch (North-Holland, New York, 1983).
[32] E. A. Stern *et al.*, Physica (Amsterdam) **208B&209B**, 117 (1995).
[33] A. I. Frenkel *et al.*, Phys. Rev. B **62**, 9364 (2000).
[34] V. Ozolins, C. Wolverton, and A. Zunger, Phys. Rev. B **58**, R5897 (1998).
[35] J. Marro *et al.*, Phys. Rev. B **12**, 2000 (1975).
[36] Y. Qi *et al.*, Phys. Rev. B **59**, 3527 (1999).
[37] B.F. Warren, *X-Ray Diffraction* (Dover Publications, Mineola, NY, 1990), p. 117.
[38] F. Hofer and P. Warbichler, Z. Metallkde Bd. **76**, 11 (1985).
[39] H.W. Sheng, G. Wilde, and E. Ma, Acta Mater. **50**, 475 (2002).
[40] H.W. Sheng, J. H. He, and E. Ma, Phys. Rev. B **65**, 184203 (2002).